iScience

CellPress
OPEN ACCESS

Article

Terahertz tunable vanadium dioxide metasurface for dynamic illusion and cloaking

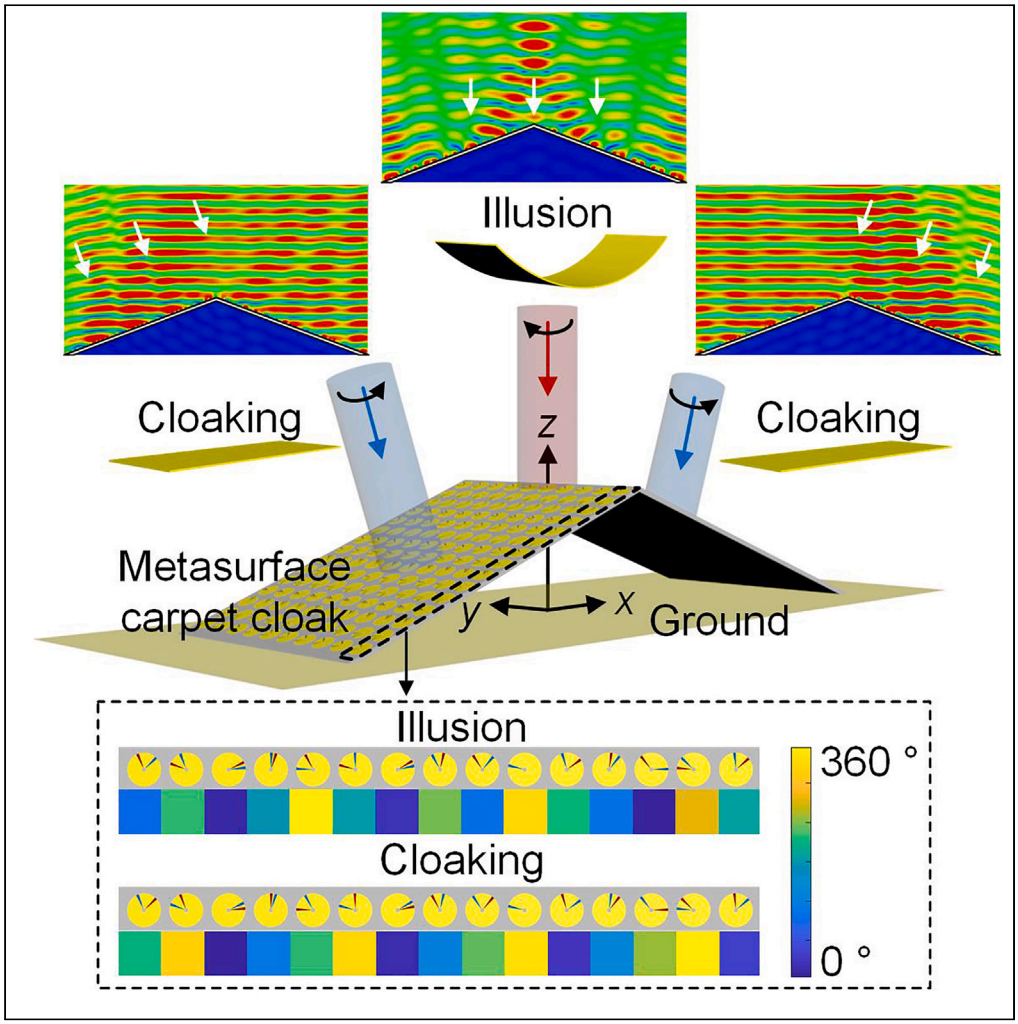

Ling Wang, Feng Gao, Shuhua Teng, Zhiguo Tan, Xing Zhang, Jun Lou

gaofeng_nudt@foxmail.com

Highlights

A terahertz tunable VO_2 metasurface for dynamic illusion and cloaking is proposed

The metasurface's function, frequency, angle, and polarization are adjustable

The metasurface is robust to the incident angle and polarization angle

Wang et al., iScience 27, 108609
January 19, 2024 © 2023 The Authors.
https://doi.org/10.1016/j.isci.2023.108609

iScience

CellPress
OPEN ACCESS

Article

Terahertz tunable vanadium dioxide metasurface for dynamic illusion and cloaking

Ling Wang,[1,2,3] Feng Gao,[1,2,*] Shuhua Teng,[1,2] Zhiguo Tan,[1,2] Xing Zhang,[1,2] and Jun Lou[1,2]

SUMMARY

Realizing camouflage by illusion and cloaking based on the metasurface has received widespread attention recently. However, existing metasurface-based illusion and cloaking devices are valid for the incident wave with a specific frequency, angle, or polarization, or exhibit a single function. Therefore, a terahertz tunable vanadium dioxide (VO_2) metasurface carpet cloak is proposed for dynamic illusion and cloaking. Simulation results show that by controlling the state of the VO_2, the metasurface carpet cloak can simultaneously achieve illusion and cloaking functions, working at 0.45 THz and 0.6 THz, and is effective for orthogonal circularly polarized waves with different incidence angles. That is the function, frequency, incident angle, and polarization of the metasurface carpet cloak are dynamically adjustable. Besides, the metasurface carpet cloak is robust to the incident angle and is capable of polarization angle stability. This work has potential value in the real-life application of metasurface-based illusion and cloaking devices.

INTRODUCTION

Camouflage technology has been investigated extensively for its aims to improve the survivability of the target. The major means for achieving camouflage include illusion and cloaking, which refer to the target's electromagnetic (EM) behavior that can mimic another object and make the target invisible in free space.[1,2] Therefore, a high enthusiasm for exploring illusion and cloaking has been maintained in modern military and civilian applications.

The emerging metasurface has provided an unprecedented ability to arbitrarily manipulate the characteristics of EM waves, such as amplitude, phase, and polarization.[3] Therefore, realizing camouflage based on the metasurface has become a reliable approach. There is some research on metasurface-based illusion and cloaking devices. The existing main illusion methods include the carpet cloak,[2,4] holography mimicry,[5–7] external cloak,[8] and perturbative metasurface.[9,10] The main cloaking design methods include the absorber,[11] carpet cloak,[12–15] mantle cloak,[16–19] and cascaded metasurfaces.[20] However, the above illusion and cloaking devices are valid for the incident EM wave with a specific frequency, angle, or polarization, exhibit a single illusion or cloaking function, are structurally complex, or can't effectively protect the target due to the planar structures. These disadvantages are obstacles to the development of metasurface-based camouflage devices.

The tunable metasurface embedded with dynamic materials or devices has attracted increasing interest recently.[21,22] Compared with ordinary metasurfaces, the tunable metasurface's performance can be easily adjusted, which enhances the flexibility and adaptability of the metasurface greatly. Some research has been done into the tunable metasurface-based illusion and cloaking devices, such as the absorber hybridized with silicon,[23] graphene,[24] and vanadium dioxide (VO_2)[25] and the metasurface cloak hybridized with the $Ge_2Sb_2Se_2Te_1$(GSST),[26] graphene,[27,28] and $Ge_2Sb_2Te_5$.[29] These devices possess the tunable absorption performance, the cloaking function, or frequency. However, the cloaking is valid for the incident wave with a specific angle and is hard to effectively protect the target. A tunable metasurface cloak embedded with the PIN diode has been proposed recently.[30] Although the metasurface is self-adaptive to the frequency and angle of the incident EM wave, the cloaking is only valid for transverse-magnetic polarized illumination. Besides, the above metasurface cloaks exhibit a single cloaking function. Recently, the tunable metasurfaces combined with the shape memory polymer[1] or the PIN diode[31,32] that can simultaneously achieve illusion and cloaking functions have been designed. However, they are still valid for the incident wave with a specific frequency, angle, or polarization. Therefore, further detailed explorations are needed.

This paper presents a terahertz tunable VO_2 metasurface carpet cloak for dynamic illusion and cloaking. The VO_2 can exhibit an insulator-to-metal transition at around 68°C.[33,34] Therefore, combining VO_2 to design the tunable metasurface is an effective means.[35,36] The designed tunable unit cell consists of the top layer split ring resonator (SRR) embedded with VO_2, middle dielectric layer, and bottom metal plate. The Pancharatnam-Berry (PB) phase is used to introduce the abrupt phase.[37,38] Unit cells are arranged according to the theoretical abrupt phase distribution to form the required metasurface carpet cloak. The simulation results indicate that by controlling the state of the VO_2, the

[1]School of Electronic Information, Hunan First Normal University, Changsha, Hunan 410205, China
[2]Key Laboratory of Hunan Province for 3D Scene Visualization and Intelligence Education, Hunan First Normal University, Changsha, Hunan 410205, China
[3]Lead contact
*Correspondence: gaofeng_nudt@foxmail.com
https://doi.org/10.1016/j.isci.2023.108609

This is an open access article under the CC BY-NC-ND license (http://creativecommons.org/licenses/by-nc-nd/4.0/).

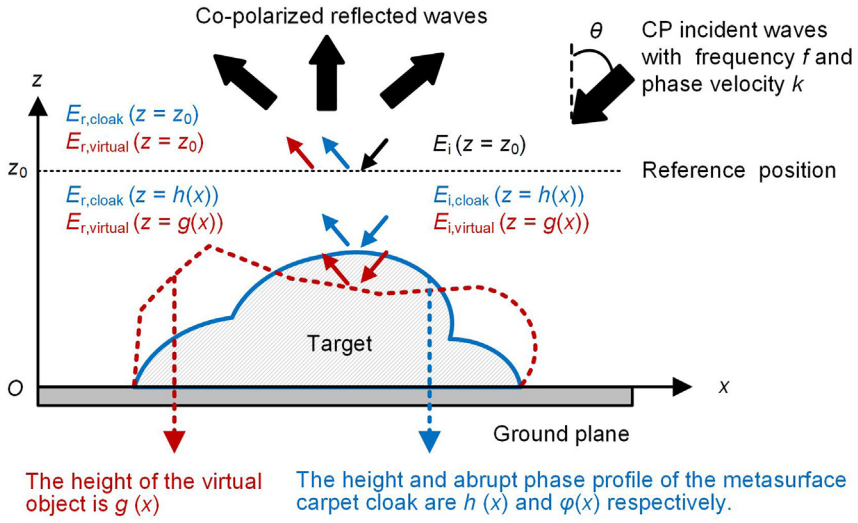

Figure 1. Working principle schematic diagram of the metasurface carpet cloak.

metasurface can implement the illusion under the right-handed circularly polarized (RCP) perpendicular incident wave with a frequency of 0.45 THz and can achieve the cloaking under the left-handed circularly polarized (LCP) oblique incident wave with a frequency of 0.6 THz and angles of $\pm 20^{\circ}$. The function, working frequency, incident angle, and polarization of the metasurface carpet cloak are dynamically adjustable. Besides, the unit cell and metasurface are robust to the incident angle and are capable of polarization angle stability. This work has potential value in the real-life application of metasurface-based illusion and cloaking devices.

RESULTS AND DISCUSSION

Design principle

Figure 1 shows the working principle schematic diagram of the metasurface carpet cloak. The metasurface's height and abrupt phase profile are $h(x)$ and $\varphi(x)$. The height of the virtual object is $g(x)$. The plane wave with the frequency f, angle θ, and phase velocity $k = 2\pi f/C$ ($C = 3 \times 10^8$ m/s is the propagation velocity of the EM wave in free space) is incident to the metasurface. Take $z = z_0$ as the reference position. First, the electric field component in the z-direction of the incident wave at $z = z_0$ can be expressed as Equation 1:

$$E_i(z = z_0) = e^{jk\cos\theta z} \quad \text{(Equation 1)}$$

Then, when the $E_i(z = z_0)$ propagates to the position of the metasurface or the virtual object, the electric field component can be expressed as Equations 2 and 3:

$$E_{i,cloak}(z = h(x)) = e^{jk\cos\theta[z-(z_0-h(x))]} = e^{jk\cos\theta z}e^{-jk\cos\theta(z_0-h(x))} \quad \text{(Equation 2)}$$

$$E_{i,virtual}(z = g(x)) = e^{jk\cos\theta[z-(z_0-g(x))]} = e^{jk\cos\theta z}e^{-jk\cos\theta(z_0-g(x))} \quad \text{(Equation 3)}$$

Next, as the abrupt phase φ can be introduced by the metasurface, for the metasurface carpet cloak, the electric field component of the reflected wave can be expressed as Equation 4:

$$\begin{aligned} E_{r,cloak}(z = h(x)) &= e^{-jk\cos\theta z}e^{-jk\cos\theta(z_0-h(x))}e^{j\varphi(x)} \\ &= e^{-jk\cos\theta z}e^{j[\varphi(x)-k\cos\theta(z_0-h(x))]} \end{aligned} \quad \text{(Equation 4)}$$

The material of the virtual object is metal. Therefore, an additional π phase jump is induced by the reflecting mirror. For the metal virtual object, the electric field component of the reflected wave can be expressed as Equation 5:

$$E_{r,virtual}(z = g(x)) = e^{-j(k\cos\theta z-\pi)}e^{-jk\cos\theta(z_0-g(x))} = e^{-jk\cos\theta z}e^{j[\pi-k\cos\theta(z_0-g(x))]} \quad \text{(Equation 5)}$$

After that, when the $E_{r,cloak}(z = h(x))$ or $E_{r,virtual}(z = g(x))$ propagates to the reference position, the electric field component of the reflected wave can be expressed as Equations 6 and 7:

$$\begin{aligned} E_{r,cloak}(z = z_0) &= e^{-jk\cos\theta[z+(z_0-h(x))]}e^{j[\varphi(x)-k\cos\theta(z_0-h(x))]} \\ &= e^{-jk\cos\theta z}e^{j[\varphi(x)-2k\cos\theta(z_0-h(x))]} \end{aligned} \quad \text{(Equation 6)}$$

$$E_{r,virtual}(z = z_0) = e^{-jk\cos\theta[z+(z_0-g(x))]}e^{j[\pi - k\cos\theta(z_0-g(x))]} = e^{-jk\cos\theta z}e^{j[\pi-2k\cos\theta(z_0-g(x))]} \quad \text{(Equation 7)}$$

Finally, to make the metasurface mimic the EM behavior of the virtual object, $E_{r,cloak}$ ($z = z_0$) and $E_{r,virtual}$ ($z = z_0$) should be equal. Therefore, the abrupt phase profile can be expressed as Equation 8:[1,2]

$$\varphi(x) = \pi - \frac{4\pi f}{C}\cos\theta[h(x) - g(x)] \quad \text{(Equation 8)}$$

Therefore, if the abrupt phase profile of the metasurface is satisfied with the $\varphi(x)$, the metasurface can mimic the EM behavior of the virtual object. The target covered by the metasurface carpet cloak can be camouflaged as a virtual object. It is worth noting that when taking $g(x) = 0$, the virtual object is the metal ground plane and the metasurface can realize the cloaking function.

The required abrupt phase profile is introduced based on the PB phase principle.[37,38] When linearly polarized (LP) EM waves illuminate a reflective unit cell with any rotation angle, the unit cell can be represented by the Jones matrix M. M can be expressed as Equation 9:[39–41]

$$M = \begin{bmatrix} \cos(2\alpha) & -\sin(2\alpha) \\ -\sin(2\alpha) & -\cos(2\alpha) \end{bmatrix} \quad \text{(Equation 9)}$$

in which α represents the rotation angle of the unit cell. The generated reflected wave can be expressed as Equation 10:

$$\begin{bmatrix} E_x \\ E_y \end{bmatrix}_{out} = M\begin{bmatrix} E_x \\ E_y \end{bmatrix}_{in} \quad \text{(Equation 10)}$$

in which x and y denote LP waves. Circularly polarized (CP) incident waves propagating in the negative z direction and CP reflective waves propagating in the positive z direction can be expressed as Equations 11 and 12:

$$\begin{bmatrix} E_L \\ E_R \end{bmatrix}_{in} = \frac{1}{\sqrt{2}}\begin{bmatrix} 1 & -j \\ 1 & j \end{bmatrix}\begin{bmatrix} E_x \\ E_y \end{bmatrix}_{in} = C_1\begin{bmatrix} E_x \\ E_y \end{bmatrix}_{in} \quad \text{(Equation 11)}$$

$$\begin{bmatrix} E_L \\ E_R \end{bmatrix}_{out} = \frac{1}{\sqrt{2}}\begin{bmatrix} 1 & j \\ 1 & -j \end{bmatrix}\begin{bmatrix} E_x \\ E_y \end{bmatrix}_{out} = C_2\begin{bmatrix} E_x \\ E_y \end{bmatrix}_{out} \quad \text{(Equation 12)}$$

in which L and R represent the LCP and RCP waves. According to the Equations 9–12, for the LP incident wave, the reflected wave can be expressed as Equation 13:

$$\begin{bmatrix} E_L \\ E_R \end{bmatrix}_{out} = C_2 M C_1^{-1}\begin{bmatrix} E_L \\ E_R \end{bmatrix}_{in} = \begin{bmatrix} e^{-j2\alpha} & 0 \\ 0 & e^{j2\alpha} \end{bmatrix}\begin{bmatrix} E_L \\ E_R \end{bmatrix}_{in} \quad \text{(Equation 13)}$$

It is thus clear that, for the LCP or RCP incident waves, the co-polarized reflected wave will carry -2α or 2α additional phases (PB phase). Therefore, the desired abrupt phase can be introduced by changing the rotation angle of the unit cell.

Equation 8 shows that the metasurface carpet cloak's abrupt phase profile $\varphi(x)$ is a function of the frequency f and incident angle θ. Besides, $\varphi(x)$ is different with varying $g(x)$. Therefore, the general metasurface carpet cloak with fixed $\varphi(x)$ works at a single frequency, specific incident angle, and polarization state. Besides, the ordinary metasurface carpet cloak can only exhibit a single illusion or cloaking function. Therefore, in this paper, VO_2 is used to realize the tunable metasurface carpet cloak for dynamic illusion and cloaking.

In the terahertz, the characteristic of the VO_2 in the insulating or metallic states can be described by the equivalent complex permittivity ε and conductivity σ. ε can be expressed as equation (14) by the Drude model[42,43]:

$$\varepsilon_c(\omega) = \varepsilon_r(\omega) + j\varepsilon_i(\omega) = \varepsilon_\infty - \frac{\omega_p^2}{\omega^2 + j\gamma\omega} \quad \text{(Equation 14)}$$

in which ω, ε_∞, $\omega_p{}^2$, and γ represent the angular frequency, permittivity at high frequency, plasma frequency, and collision frequency. σ can be expressed as Equation 15 by the Drude model:

$$\sigma(\omega) = \frac{j\varepsilon_0\omega_p^2}{\omega + j\gamma} \quad \text{(Equation 15)}$$

in which $\omega_p{}^2$ can be approximately expressed as Equation 16:

$$\omega_p^2(\sigma) = \frac{\sigma}{\sigma_0}\omega_p^2(\sigma_0) \quad \text{(Equation 16)}$$

$\omega_p{}^2(\sigma_0) = 1.4 \times 10^{15}$ rad/s, $\sigma_0 = 3 \times 10^3\ \Omega^{-1}\text{cm}^{-1}$, and $\gamma = 5.75 \times 10^{13}\ \text{s}^{-1}$ with $\varepsilon_\infty = 12$. For VO_2 in the insulating and metallic states, set σ to 200 S/m and 2×10^5 S/m. Besides, when VO_2 is insulating, as σ and $\omega_p{}^2$ are small, ε is approximately ε_∞.

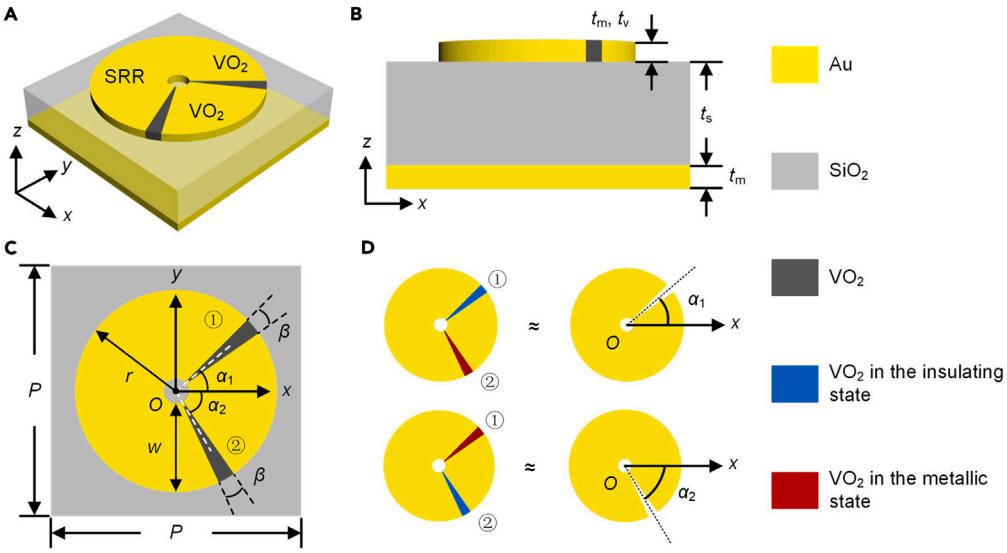

Figure 2. Diagram of the tunable unit cell embedded with VO_2 patches

(A) 3D stereogram.

(B) Side view.

(C) Vertical view.

(D) The approximate equivalent structure of the top layer with VO_2 patches in different states. t_m = 0.2 μm, t_v = 0.2 μm, t_s = 35 μm, p = 200 μm, r = 80 μm, w = 70 μm, and β = 10°.

Unit cell

Figure 2 shows the schematic of the tunable unit cell. The proposed tunable unit cell consists of three layers. From top to bottom: the SRR is embedded with two fan-shaped VO_2 patches, the dielectric layer, and the metal plate. To distinguish the two VO_2 patches, label the first and second patches as ① and ②. The metal is gold (Au) with a 4.561 × 10^7 S/m conductivity. The dielectric layer is silica (SiO_2) with a 3.8 relative permittivity. According to the LC equivalent circuit theory, the performance of the SRR is mainly affected by the thickness t_m, opening radian β, radius r, and width w.[44] After optimizing (Refer to the supplemental information S1 for details), the thicknesses of the gold, VO_2, and SiO_2 are 0.2 μm, 0.2 μm, and 35 μm. The period P of the unit cell is 200 μm. The radius r and width w of the SRR are 80 μm and 70 μm. The radian β of VO_2 patches is 10°, and the angles between VO_2 patches and the positive x-axis are α_1 and α_2. VO_2 patches can exhibit insulator-to-metal transition. Figure 2D shows the approximate equivalent structures of the SRR. When patch ② or ① is in the metallic state and patch ① or ② is insulating, varying α_1 or α_2 can acquire the expected PB phases.

Simulate the devised unit cell in the CST Studio Suite 2022. Apply the Frequency Domain Solver. Set boundary conditions as the unit cell in the x- and y-directions. Set two Floquet ports in the z-direction. The port excitation is the CP plane wave. VO_2 is simulated based on the Drude model with ε_∞ = 12, ω_p^2 (σ_0) = 1.4 × 10^{15} rad/s, σ_0 = 3 × 10^3 Ω^{-1}cm^{-1}, and γ = 5.75 × 10^{13} s^{-1}. For VO_2 in the state of insulation or metal, set σ to 200 S/m or 2 × 10^5 S/m.

To verify, first, set VO_2 patches ① and ② to the state of insulation or metal. Take α_2 = −140° and α_1 vary from 0° to 180° with a step of 30° as an example. When the RCP wave is perpendicularly incident to the unit cell along the negative z-direction, Figure 3 shows the simulation result of the co-polarized reflection coefficient R_{RR}. Figure 3A shows that the phase of R_{RR} gradually increases with α_1 changing and the phase curves remain parallel. Besides, the amplitude of R_{RR} is above 0.7 dB in the range of 0.45 THz to 0.6 THz. Take 0.45 THz as an example. According to Figure 3B, the PB phase is approximately $2\alpha_1$ and can cover 0°–360° by varying α_1 from 0° to 180° and. In addition, the amplitude of R_{RR} is above 0.8 dB. The cross-polarized reflection coefficient is below 0.1 dB. Therefore, the simulation results are consistent with the PB phase principle. When VO_2 patches ① and ② are insulating and metallic, rotating the VO_2 patch ① can introduce the desired abrupt phase while maintaining high efficiency.

Next, set VO_2 patches ① and ② in the metallic and insulating states. Take α_1 = 150° and α_2 vary from 0° to −180° with a step of −30° as an example. When the LCP wave is obliquely incident to the unit cell along the negative z-direction at an angle of 20°, Figure 4 shows the simulation result of the co-polarized reflection coefficient R_{LL}. According to Figure 4A, it also can be seen that the phase of R_{LL} gradually increases with α_2 changing and the phase curves remain parallel. Besides, the amplitude of R_{LL} is above 0.7 dB at the range of 0.45 THz to 0.6 THz. Take 0.6 THz as an example. According to Figure 4B, the PB phase is approximately $-2\alpha_2$ and can cover 0°–360° by varying α_2 from 0° to −180°. In addition, the amplitude is above 0.75 dB. The cross-polarized reflection coefficient is below 0.2 dB. Therefore, the simulation results are consistent with the PB phase principle. When VO_2 patches ① and ② are metallic and insulating, rotating the VO_2 patch ② can obtain the desired abrupt phase while maintaining high efficiency.

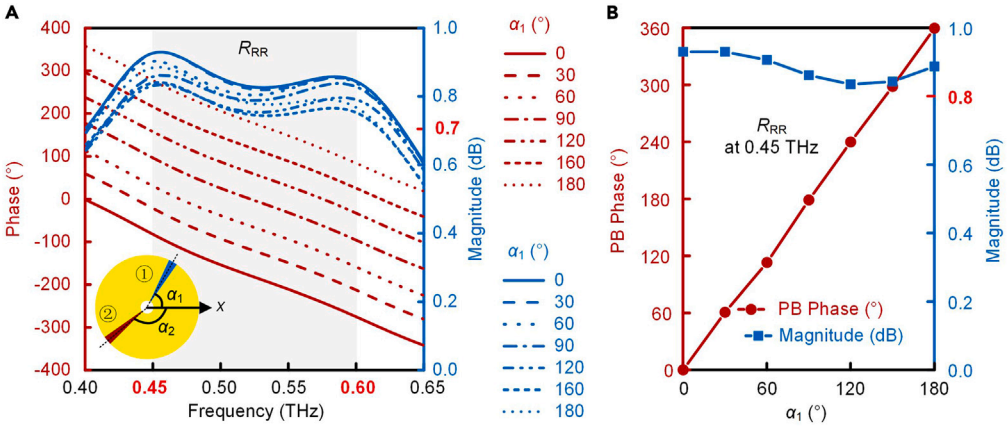

Figure 3. For the RCP perpendicular incident wave along the negative *z*-direction, when $\alpha_2 = -140^\circ$ and α_1 varies from 0° to 180° with a step of 30°, the simulation result of the co-polarized reflection coefficient R_{RR}

(A) The phase and amplitude of R_{RR} at the range of 0.4 THz to 0.65 THz.

(B) The PB phase and amplitude of R_{RR} at 0.45 THz.

Metasurface

A terahertz tunable metasurface hybridized with VO_2 for dynamic illusion and cloaking is designed for verification. Figure 5 shows the schematic diagram of the working principle. When VO_2 patches ① and ② are insulating and metallic, for RCP plane waves perpendicularly incident along the negative *z*-direction with $f = 0.45$ THz and $\theta = 0^\circ$, the metasurface can mimic the EM behavior of the arc-shaped metal depression and achieve the illusion function. When VO_2 patches ① and ② are metallic and insulating, for LCP plane waves obliquely incident along the negative *z*-direction with $f = 0.6$ THz and $\theta = \pm 20^\circ$, the metasurface can mimic the EM behavior of the metal ground plane and achieve the cloaking function. The metasurface is composed of 30 × 10 unit cells. The illustration in the lower shows the schematic diagram of the metasurface structure and the corresponding phase distribution. As shown in Figure 6, the cross-section of the metasurface carpet cloak is triangular. The tilt angle η is 20°. The triangle's length L and height H are approximately 5638 μm and 1026 μm $h(x)$, $g_i(x)$, and $g_c(x)$ denote metasurface carpet cloak and virtual objects in the *z*-direction. For the illusion, $g_i(x)$ is a circular arc depression with a radius of R. For the cloaking, $g_c(x) = 0$.

Simulate the devised tunable metasurface carpet cloak in the CST Studio Suite. Besides, the bared triangular metal bump and the virtual objects (including the arc-shaped metal depression and metal ground plane) are simulated for comparison. Apply the Time Domain Solver. Set boundary conditions as periodic in the *y*-direction and open in the *x*- and *z*-directions. The CP plane wave illuminates the metasurface, metal bump, and virtual objects in the negative *z*-direction. When the metasurface carpet cloak operates on the illusion function, Figure 7 shows the simulated average value of the total near electric field's *x* component. For the RCP incident wave

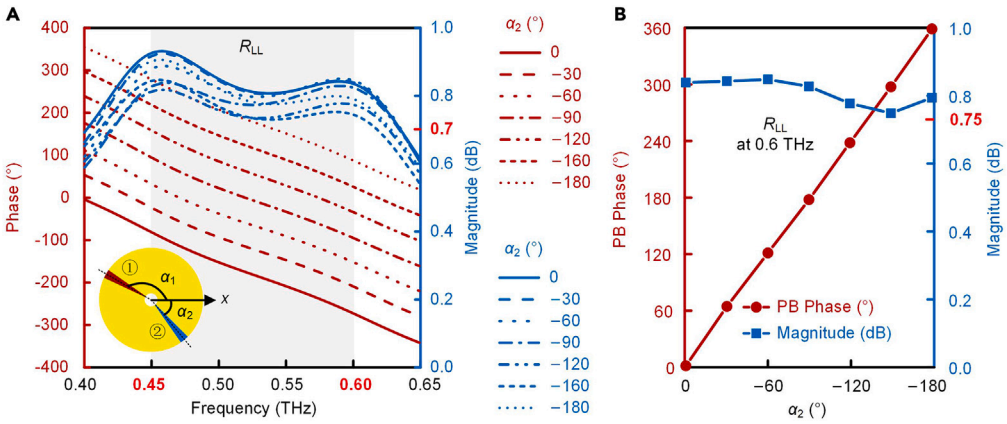

Figure 4. For the LCP oblique incident wave along the negative *z*-direction at an angle of 20°, when $\alpha_1 = 150^\circ$ and α_2 varies from 0° to −180° with a step of −30°, the simulation result of the co-polarized reflection coefficient R_{LL}

(A) The phase and amplitude of R_{LL} at the range of 0.4 THz to 0.65 THz.

(B) The PB phase and amplitude of R_{LL} at 0.6 THz.

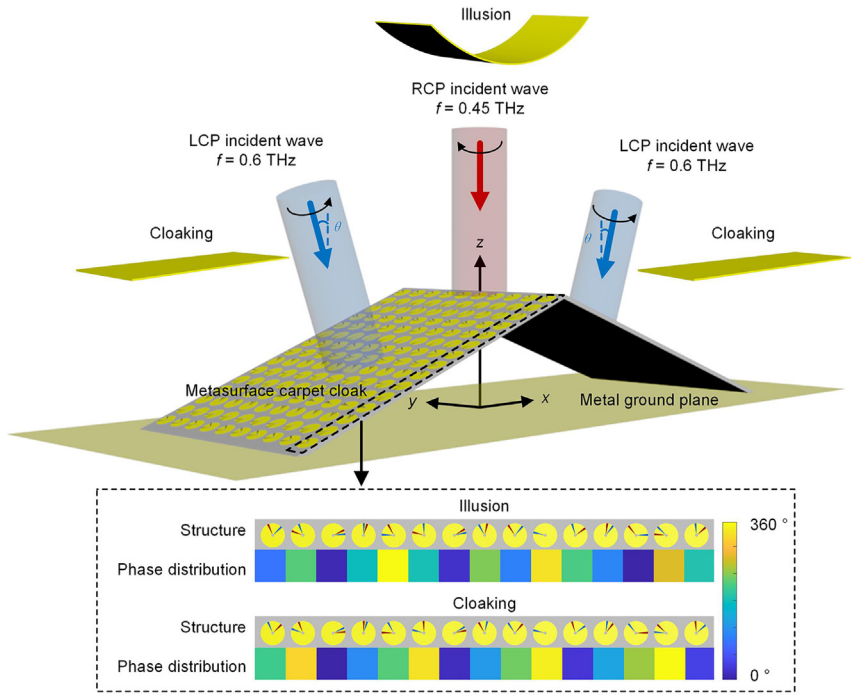

Figure 5. Diagram of the working principle of the proposed metasurface carpet cloak

When VO_2 patches ① and ② are insulating and metallic, the metasurface can achieve the illusion function under RCP plane waves perpendicularly incident along the negative *z*-direction with $f = 0.45$ THz and $\theta = 0°$. When VO_2 patches ① and ② are metallic and insulating, the metasurface can achieve the cloaking function under LCP plane waves obliquely incident along the negative *z*-direction with $f = 0.6$ THz and $\theta = \pm 20°$.

with $f = 0.45$ THz and $\theta = 0°$, the total near-field distributions of the arc-shaped metal depression and bared triangular metal bump are shown in Figures 7A–7D show the total near-field distributions of the metasurface carpet cloak under the LCP and RCP incident waves with $f = 0.45$ THz and $\theta = 0°$. Figure 8 shows the corresponding absolute value of the radar cross section (RCS). The range of the polar angle θ_p is 0°–90° and the azimuth angle $\varphi_a = 0°$ and 180°. The contrast of Figures 7A, 7D, 8A, and 8D show that the metasurface can mimic the scattered field of the arc-shaped metal depression. Therefore, the metasurface carpet cloak can achieve the illusion function under the RCP wave with $f = 0.45$ THz and $\theta = 0°$.

When the metasurface carpet cloak operates on the cloaking function, Figures 9, 10, 11, and 12 show the simulated average value of the total near electric field' *x* component and the corresponding absolute value of the RCS. For the LCP incident wave with $f = 0.6$ THz and $\theta = \pm 20°$, Figures 9A, 9B, 11A, and 11B show the total near-field distributions of the metal ground plane and bared triangular metal bump. For the LCP and RCP incident waves with $f = 0.6$ THz and $\theta = \pm 20°$, Figures 9C, 9D, 11C, and 11D show the total near-field distributions of the

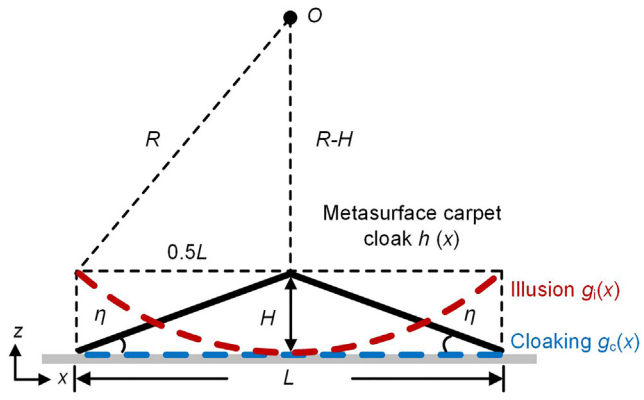

Figure 6. The cross-section of the carpet cloak, illusion, and cloaking.

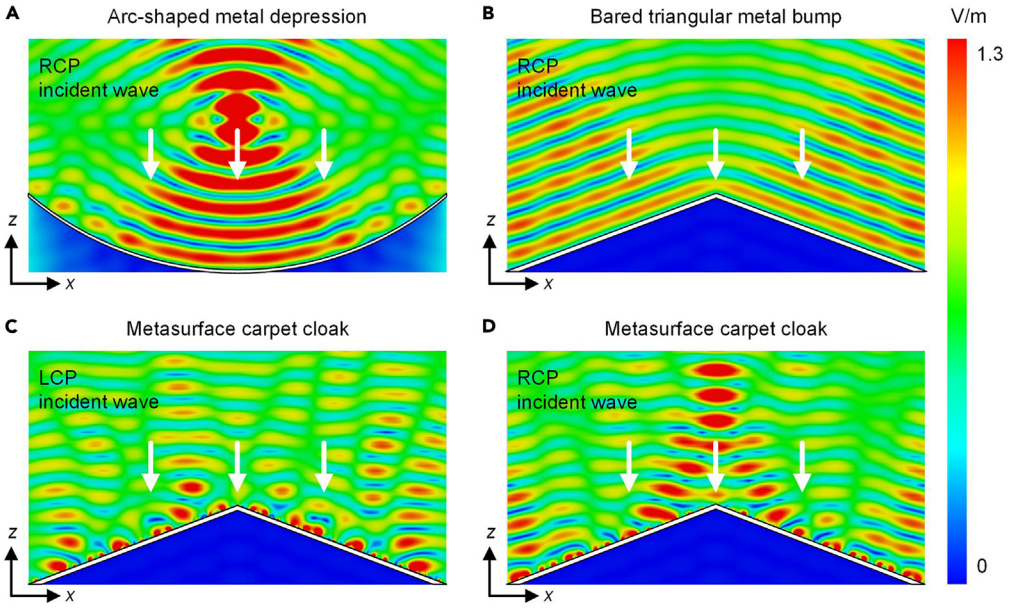

Figure 7. For the CP incident wave along the negative *z*-direction with $f = 0.45$ THz and $\theta = 0^\circ$, the simulated average value of the total near electric field's *x* component

(A–D) When the RCP plane wave illuminates (A) the arc-shaped metal depression and (B) the bared triangular metal bump. When (C) the LCP plane wave and (D) the RCP plane wave illuminates the carpet cloak.

metasurface carpet cloak. The range of the polar angle θ_p is 0°–90° and the azimuth angle $\varphi_a = 0^\circ$ and 180°. The contrast of Figures 9A, 9C, 10A, 10C, 12A, and 12C show that the metasurface can mimic the scattered field of the metal ground plane. Therefore, the metasurface carpet cloak can achieve the cloaking function under the LCP wave with $f = 0.6$ THz and $\theta = \pm 20^\circ$.

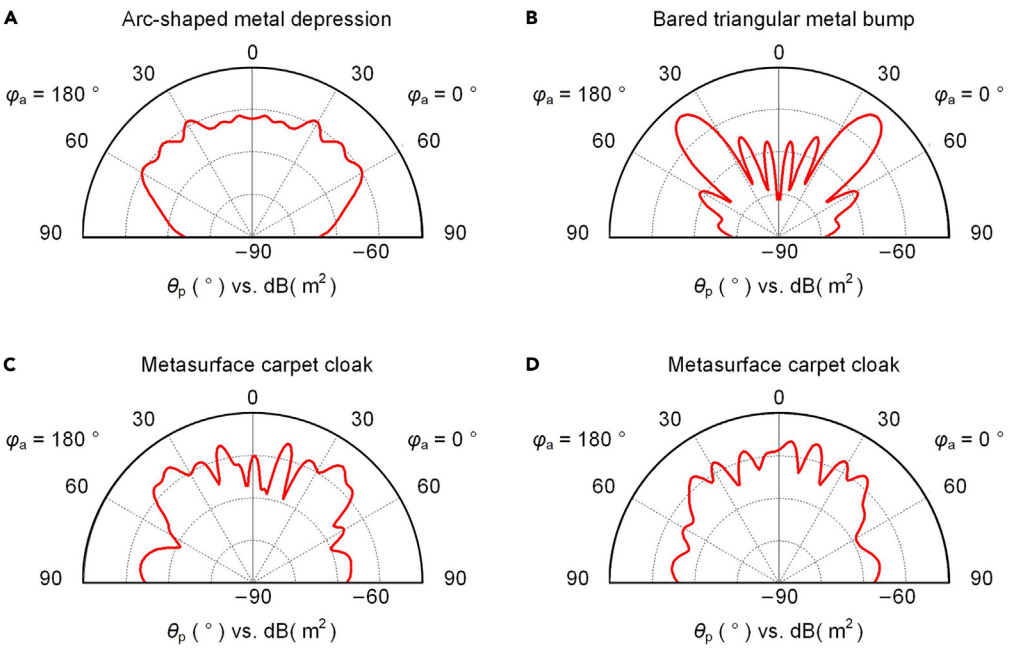

Figure 8. The corresponding absolute value of the RCS with $\theta_p = 0^\circ$–90° and $\varphi_a = 0^\circ$ and 180°

(A–D) When the RCP plane wave illuminates (A) the arc-shaped metal depression and (B) the bared triangular metal bump. When (C) the LCP plane wave and (D) the RCP plane wave illuminates the carpet cloak.

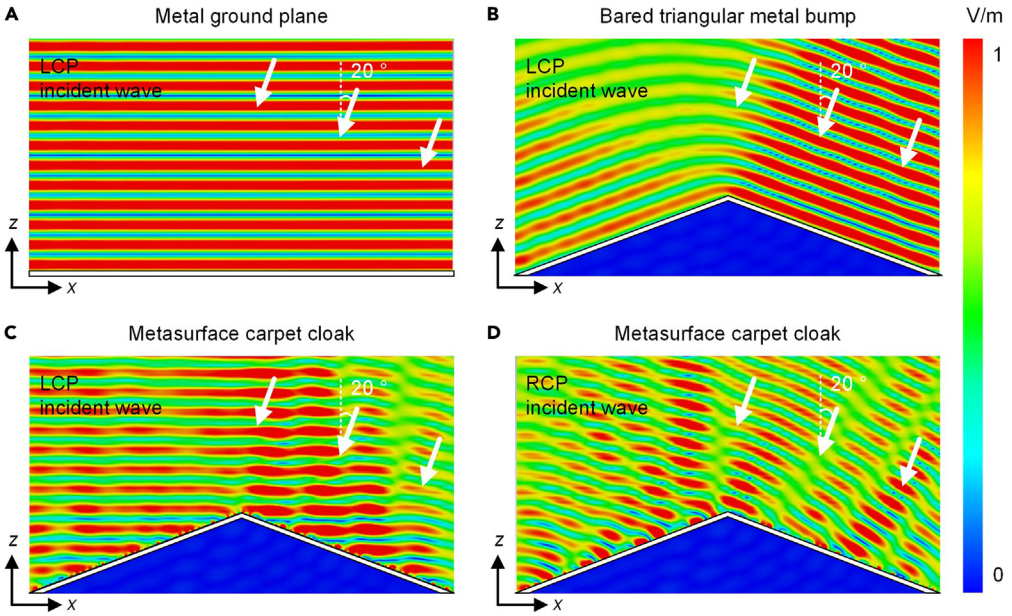

Figure 9. For the CP incident wave along the negative *z*-direction with $f = 0.6$ THz and $\theta = 20^{\circ}$, the simulated average value of the total near electric field's *x* component

When the LCP plane wave illuminates (A) the metal ground plane and (B) the bared triangular metal bump. When (C) the LCP wave and (D) the RCP plane wave illuminates the carpet cloak.

The above results show that the function, working frequency, incident angle, and polarization of the terahertz metasurface carpet cloak are dynamically adjustable. The dynamic illusion and cloaking can be realized based on the metasurface carpet cloak.

Incident angle and polarization angle stability

To further investigate the properties of the designed metasurface carpet cloak, the metasurface under varying incident angles and polarization angles are simulated (Refer to the supplemental information S2 for details). Figures S4–S11 show that the illusion function is sensitive to the incident angle, and the cloaking function is robust to the incident angle. Figures S12–S21 show that the illusion and cloaking function is insensitive to the polarization angle. The metasurface is capable of polarization angle stability.

Conclusion

A terahertz tunable VO_2 metasurface carpet cloak for dynamic illusion and cloaking is proposed in this paper. The unit cell consists of a top layer SRR embedded with two fan-shaped VO_2 patches, a middle SiO_2 layer, and a bottom Au plate. Rotating VO_2 patches and switching the VO_2 patches between the insulating and metallic states can achieve different phase responses. A metasurface carpet cloak containing 30 × 10 unit cells is devised for verification. Simulation results show that the metasurface can realize the illusion function under the RCP plane wave with $f = 0.45$ THz and $\theta = 0^{\circ}$. The metasurface can realize the cloaking function under the LCP plane wave with $f = 0.6$ THz and $\theta = \pm 20^{\circ}$. Therefore, the designed metasurface can achieve illusion and cloaking functions, operate in 0.45 THz and 0.6 THz, and is valid for RCP perpendicular and LCP oblique incident waves. The function, working frequency, incident angle, and polarization of the metasurface carpet cloak are dynamically adjustable. Dynamic illusion and cloaking can be realized based on the metasurface carpet cloak. Besides, the metasurface carpet cloak is robust to the incident angle and is capable of polarization angle stability. The designed metasurface carpet cloak has potential application in the modern military and civilian. The proposed method has potential value in the real-life application of metasurface-based illusion and cloaking devices.

Limitations of the study

The fabrication and performance measurements are the key challenges because of the lack of experimental conditions. Our future studies may focus on these. According to the previous work, photolithography may be used to fabricate the proposed metasurface. The possible manufacturing procedures are as follows: (1) Deposit Au onto a silicon wafer as the bottom plate. (2) Spin SiO_2 onto the Au layer as the middle dielectric layer. (3) Spin coat and deposit the photoresist on the SiO_2 layer and pattern the photoresist. (4) Deposit VO_2 and dissolve the photoresist to form the fan-shaped VO_2 patch. (5) Spin coat and pattern the photoresist. (6) Deposit Au and dissolve the photoresist to form the SRR. Testing the near-field amplitude using the THz imaging system could verify

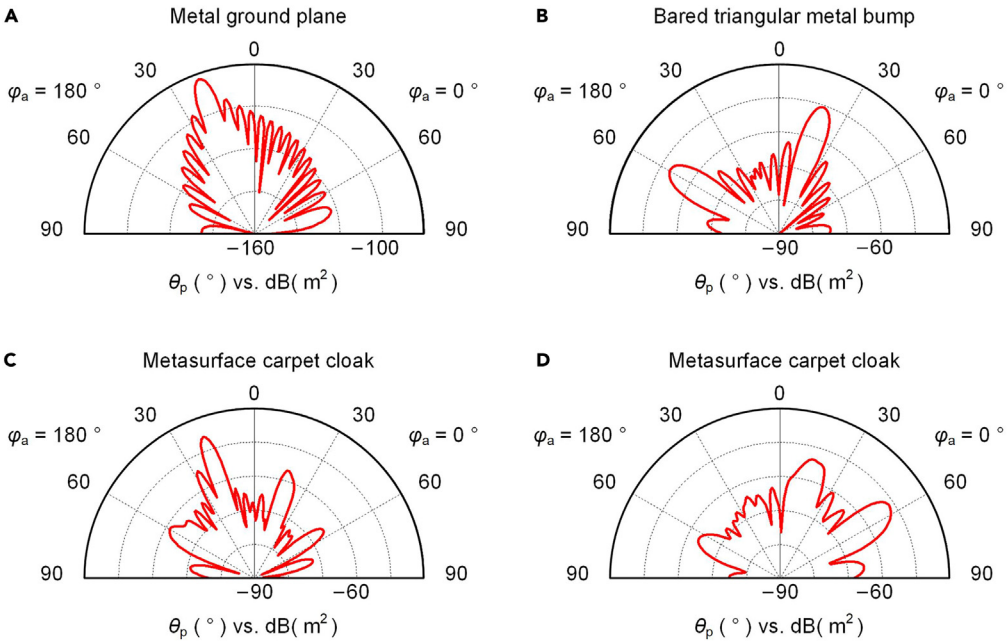

Figure 10. The corresponding absolute value of the RCS with θ_p = 0°–90° and φ_a = 0° and 180°

(A–D) When the LCP plane wave illuminates (A) the metal ground plane and (B) the bared triangular metal bump. When (C) the LCP wave and (D) the RCP plane wave illuminates the carpet cloak.

the performance. The switching of the VO_2 state could be realized by heating (Refer to the supplemental information S3 for details).[35,42,45]

STAR★METHODS

Detailed methods are provided in the online version of this paper and include the following:

- KEY RESOURCES TABLE
- RESOURCE AVAILABILITY
  - Lead contact
  - Materials availability
  - Data and code availability
- EXPERIMENTAL MODEL AND SUBJECT DETAILS
- METHOD DETAILS
- QUANTITATION AND STATISTICAL ANALYSIS
- ADDITIONAL RESOURCES

SUPPLEMENTAL INFORMATION

Supplemental information can be found online at https://doi.org/10.1016/j.isci.2023.108609.

ACKNOWLEDGMENTS

This work was supported by the Natural Science Foundation of Hunan Province (Grant Nos. 2022JJ40114 and 2023JJ30185), the Research Foundation of Education Bureau of Hunan Province (Grant Nos. 22A0640 and 21B0811), and Key Laboratory of Hunan Province for 3D Scene Visualization and Intelligence Education (Grant No. 2023TP1038).

AUTHOR CONTRIBUTIONS

L.W.: Conceptualization, Methodology, Software, Validation, Writing – Original Draft, Writing - Review and Editing. F.G.: Resources, Supervision, Writing - Review and Editing. S.T.: Resources, Supervision, Writing – Review and Editing. Z.T.: Methodology, Writing - Review and Editing. X.Z.: Methodology, Writing – Review and Editing. J.L.: Methodology, Writing – Review and editing.

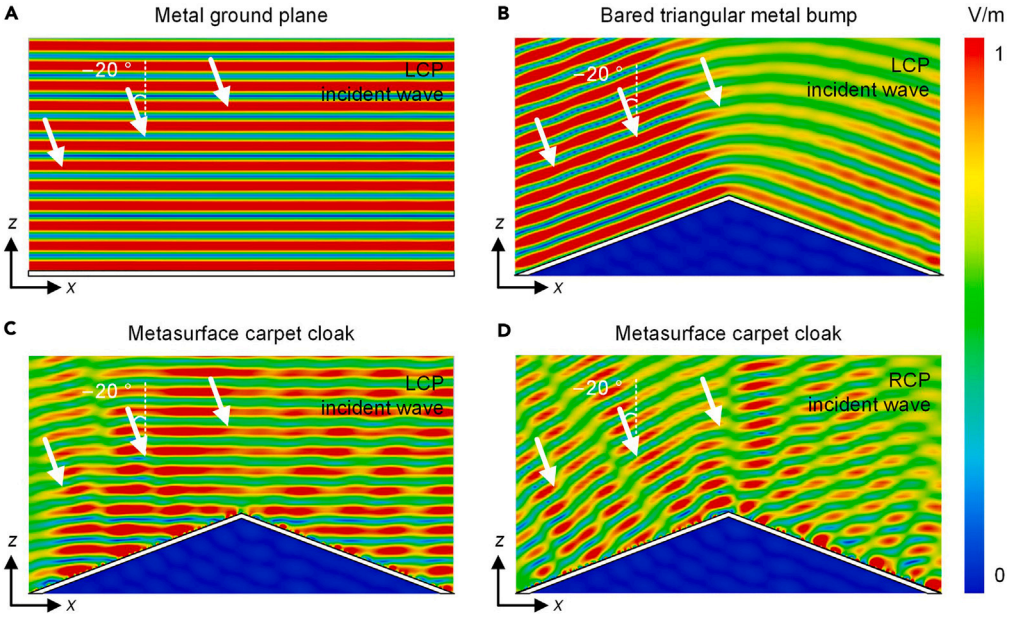

Figure 11. For the CP incident wave along the negative *z*-direction with *f* = 0.6 THz and $\theta = -20^{\circ}$, the simulated average value of the total near electric field's *x* component

(A–D) When the LCP plane wave illuminates (A) the metal ground plane and (B) the bared triangular metal bump. When (C) the LCP plane wave and (D) the RCP plane wave illuminates the carpet cloak.

DECLARATION OF INTERESTS

The authors declare no conflicts of interest.

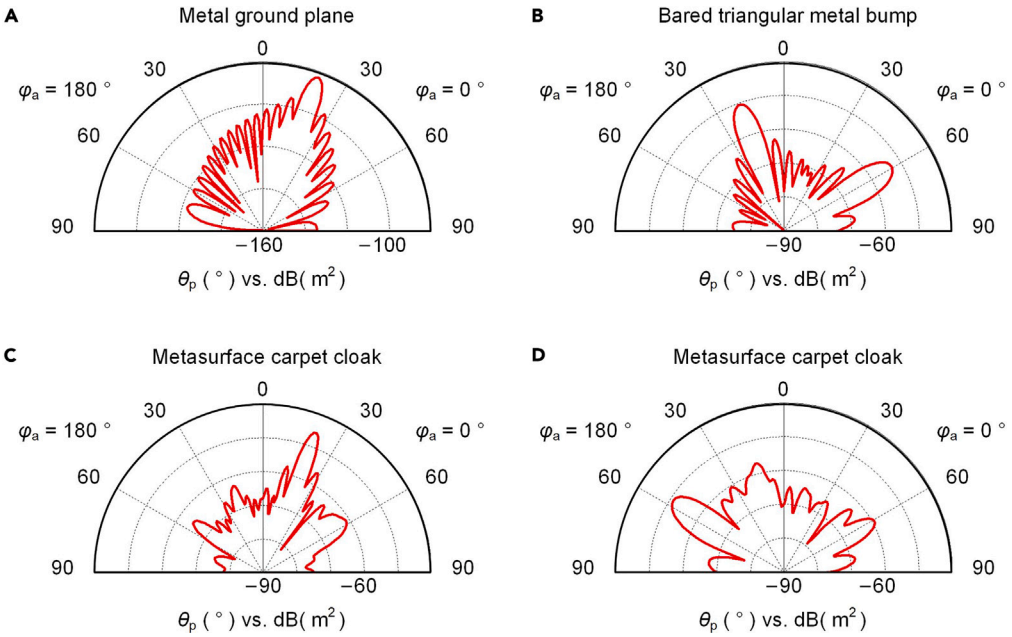

Figure 12. The corresponding absolute value of the RCS with $\theta_p = 0^{\circ}$–90° and $\varphi_a = 0^{\circ}$ and 180°

(A–D) When the LCP plane wave illuminates (A) the metal ground plane and (B) the bared triangular metal bump. When (C) the LCP plane wave and (D) the RCP plane wave illuminates the carpet cloak.

Received: August 21, 2023
Revised: November 22, 2023
Accepted: November 29, 2023
Published: November 30, 2023

REFERENCES

1. Liang, Q., Li, Z., Xu, J., Duan, Y., Yang, Z., and Li, D. (2023). A 4D-Printed Electromagnetic Cloaking and Illusion Function Convertible Metasurface. Adv. Mater. Technol. *2202020*.
2. Liang, Q., Li, Z., Jiang, Z., Duan, Y., Chen, T., and Li, D. (2020). A 3D-printed adaptive cloaking–illusion-integrated metasurface. J. Mater. Chem. C *8*, 16018–16023.
3. Hu, J., Bandyopadhyay, S., Liu, Y.H., and Shao, L.Y. (2021). A review on metasurface: from principle to smart metadevices. Front. Phys. *8*, 586087.
4. Jia, Y., Qian, C., Fan, Z., Ding, Y., Wang, Z., Wang, D., Li, E.P., Zheng, B., Cai, T., and Chen, H. (2022). In situ customized illusion enabled by global metasurface reconstruction. Adv. Funct. Mater. *32*, 2109331.
5. Xiong, B., Xu, Y., Wang, J., Li, L., Deng, L., Cheng, F., Peng, R.W., Wang, M., and Liu, Y. (2021). Realizing colorful holographic mimicry by metasurfaces. Adv. Mater. *33*, 2005864.
6. Cai, H., Dolan, J.A., Gordon, G.S.D., Chung, T., and López, D. (2021). Polarization-insensitive medium-switchable holographic metasurfaces. ACS Phot. *8*, 2581–2589.
7. Smy, T.J., Stewart, S.A., and Gupta, S. (2020). Surface susceptibility synthesis of metasurface holograms for creating electromagnetic illusions. IEEE Access *8*, 93408–93425.
8. Bai, G.D., Ma, Q., Iqbal, S., Bao, L., Jing, H.B., Zhang, L., WU, H.T., Wu, R.Y., Zhang, H.C., Yang, C., and Cui, T.J. (2018). Multitasking shared aperture enabled with multiband digital coding metasurface. Adv. Opt. Mater. *6*, 1800657.
9. Huang, K., Zhao, D., Tjiptoharsono, F., Chen, Y., Wong, C.P.Y., Tang, X., Yang, J.K.W., and Dong, Z. (2020). Bio-inspired photonic masquerade with perturbative metasurfaces. ACS Nano *14*, 7529–7537.
10. Xue, J., Zhou, Z.K., Lin, L., Guo, C., Sun, S., Lei, D., Qiu, C.W., and Wang, X.H. (2019). Perturbative countersurveillance metaoptics with compound nanosieves. Light Sci. Appl. *8*, 101.
11. Qu, J., Pan, H., Sun, Y.Z., and Zhang, H.F. (2022). Multitasking Device Regulated by the Gravity Field: Broadband Anapole-Excited Absorber and Linear Polarization Converter. Ann. Phys. (Berlin) *534*, 2200175.
12. Xu, H.X., Wang, Y., Wang, C., Wang, M., Wang, S., Ding, F., Huang, Y., Zhang, X., Liu, H., Ling, X., and Huang, W. (2021). Deterministic approach to achieve full-polarization cloak. Research *2021*, 6382172.
13. Xu, H.X., Hu, G., Wang, Y., Wang, C., Wang, M., Wang, S., Huang, Y., Genevet, P., Huang, W., and Qiu, C.W. (2021). Polarization-insensitive 3D conformal-skin metasurface cloak. Light Sci. Appl. *10*, 75.
14. Yuan, X., He, Z., Ye, X., Chen, M., Li, Y., Li, W., Zhang, R., Huang, Y., Liu, C., Cheng, X., and Fang, D. (2021). Invisible electromagnetic Huygens' metasurface operational in wide frequency band and its experimental validation. IEEE Trans. Antennas Propag. *69*, 3341–3348.
15. Jiang, Z., Liang, Q., Li, Z., Chen, T., Li, D., and Hao, Y. (2020). A 3D Carpet Cloak with Non-Euclidean Metasurfaces. Adv. Opt. Mater. *8*, 2000827.
16. Younesiraad, H., Hamzavi-Zarghani, Z., and Matekovits, L. (2021). Invisibility utilizing Huygens' metasurface based on mantle cloak and scattering suppression phenomen. IEEE Trans. Antennas Propag. *69*, 5181–5186.
17. Ang, P., Xu, G., and Eleftheriades, G.V. (2021). Invisibility cloaking with passive and active Huygens's metasurfaces. Appl. Phys. Lett. *118*, 071903.
18. Kwon, D.H. (2020). Illusion electromagnetics for free-standing objects using passive lossless metasurfaces. Phys. Rev. B *101*, 235135.
19. Xu, G., Eleftheriades, G.V., and Hum, S.V. (2020). Approach to the analysis and synthesis of cylindrical metasurfaces with noncircular cross sections based on conformal transformations. Phys. Rev. B *102*, 245305.
20. Zhen, Z., Qian, C., Jia, Y., Fan, Z., Hao, R., Cai, T., Zheng, B., Chen, H., and Li, E. (2021). Realizing transmitted metasurface cloak by a tandem neural network. Photonics Res. *9*, B229–B235.
21. Zhou, Z., and Song, Z. (2022). Terahertz mode switching of spin reflection and vortex beams based on graphene metasurfaces. Opt. Laser Technol. *153*, 108278.
22. He, C., and Song, Z. (2022). Terahertz graphene metasurfaces for cross-polarized deflection, focusing, and orbital angular momentum. Opt Express *30*, 25498–25508.
23. Liao, S., Sui, J., and Zhang, H. (2022). Switchable ultra-broadband absorption and polarization conversion metastructure controlled by light. Opt Express *30*, 34172–34187.
24. Liu, W., Xu, J., and Song, Z. (2021). Bifunctional terahertz modulator for beam steering and broadband absorption based on a hybrid structure of graphene and vanadium dioxide. Opt Express *29*, 23331–23340.
25. Sun, Y.Z., Gao, C.J., Qu, J., and Zhang, H.F. (2022). Circularly Polarized Manipulations with VO_2-Doped Dielectric Electromagnetically Induced Transparency and Absorption. Ann. Phys. (Berlin) *534*, 2200130.
26. Tian, X., Xu, J., Xiao, T.H., Ding, P., Xu, K., Du, Y., and Li, Z.Y. (2022). Broadband generation of polarization-immune cloaking via a hybrid phase-change metasurface. Photonics *9*, 156.
27. Ding, P., Li, M., Tian, X., Li, Y., Shao, L., Xu, K., Huo, H., Zeng, F., and Wang, J. (2021). Graphene metasurface for broadband, wide-angle and polarization-insensitive carpet cloak. Opt. Mater. *121*, 111578.
28. Lv, C., Ding, P., Tian, X., Li, Y., Shao, L., Zeng, F., and Wang, J. (2020). Broadband and wide-angle terahertz carpet cloaks based on patterned graphene metasurfaces. J. Phys. D Appl. Phys. *53*, 155107.
29. Tian, X., Xu, J., Xu, K., Qian, Y., Ma, X., Yang, P., Duan, X., Ding, P., and Li, Z.Y. (2021). Phase-change tunable metasurface for broadband, wide-angle, continuously tunable and switchable cloaking. Opt Express *29*, 5959–5971.
30. Qian, C., Zheng, B., Shen, Y., Jing, L., Li, E., Shen, L., and Chen, H. (2020). Deep-learning-enabled self-adaptive microwave cloak without human intervention. Nat. Photonics *14*, 383–390.
31. Liao, J., Ji, C., Yuan, L., Huang, C., Wang, Y., Peng, J., and Luo, X. (2023). Polarization-Insensitive Metasurface Cloak for Dynamic Illusions with an Electromagnetic Transparent Window. ACS Appl. Mater. Interfaces *15*, 16953–16962.
32. Zhang, X.G., Jiang, W.X., Jiang, H.L., Wang, Q., Tian, H.W., Bai, L., Luo, Z.J., Sun, S., Luo, Y., Qiu, C.W., and Cui, T.J. (2020). An optically driven digital metasurface for programming electromagnetic functions. Nat. Electron. *3*, 165–171.
33. Shi, Q., Huang, W., Zhang, Y., Yan, J., Zhang, Y., Mao, M., Zhang, Y., and Tu, M. (2011). Giant phase transition properties at terahertz range in VO_2 films deposited by sol–gel method. ACS Appl. Mater. Interfaces *3*, 3523–3527.
34. Ren, Z., Xu, J., Liu, J., Li, B., Zhou, C., and Sheng, Z. (2022). Active and smart terahertz electro-optic modulator based on VO_2 structure. ACS Appl. Mater. Interfaces *14*, 26923–26930.
35. Liu, M., Hwang, H.Y., Tao, H., Strikwerda, A.C., Fan, K., Keiser, G.R., Sternbach, A.J., West, K.G., Kittiwatanakul, S., Lu, J., et al. (2012). Terahertz-field-induced insulator-to-metal transition in vanadium dioxide metamaterial. Nature *487*, 345–348.
36. Yang, D., Wang, W., Lv, E., Wang, H., Liu, B., Hou, Y., and Chen, J.H. (2022). Programmable VO_2 metasurface for terahertz wave beam steering. iScience *25*, 104824.
37. Pancharatnam, S. (1956). Generalized theory of interference, and its applications. Proc. Indian Acad. Sci. *44*, 247–262.
38. Berry, M.V. (1984). Quantal phase factors accompanying adiabatic changes. In Proceedings of the Royal Society of London. A. Mathematical and Physical Sciences, *392*Proceedings of the Royal Society of London. A. Mathematical and Physical Sciences, pp. 45–57.
39. Bomzon, Z., Biener, G., Kleiner, V., and Hasman, E. (2002). Space-variant Pancharatnam–Berry phase optical elements with computer-generated subwavelength gratings. Opt. Lett. *27*, 1141–1143.
40. Zheng, S., Li, Y., Lin, Q., Zeng, X., Zheng, G., Cai, Y., Chen, Z., Xu, S., and Fan, D. (2018). Experimental realization to efficiently sort vector beams by polarization topological charge via Pancharatnam–Berry phase modulation. Photonics Res. *6*, 385–389.

41. Xu, H.X., Wang, G.M., Cai, T., Xiao, J., and Zhuang, Y.Q. (2016). Tunable Pancharatnam–Berry metasurface for dynamical and high-efficiency anomalous reflection. Opt Express *24*, 27836–27848.
42. Kou, W., Shi, W., Zhang, Y., Yang, Z., Chen, T., Gu, J., Zhang, X., Shi, Q., Liang, S., Lan, F., et al. (2022). Terahertz switchable focusing planar lens with a nanoscale vanadium dioxide integrated metasurface. IEEE Trans. Terahertz Sci. Technol. *12*, 13–22.
43. Liu, X., Wang, Q., Zhang, X., Li, H., Xu, Q., Xu, Y., Chen, X., Li, S., Liu, M., Tian, Z., et al. (2019). Thermally dependent dynamic meta-holography using a vanadium dioxide integrated metasurface. Adv. Opt. Mater. *7*, 1900175.
44. Ortiz, J.D., Baena, J.D., Marqués, R., Enemuo, A.N., Gollub, J., Akhmechet, R., Penkov, B., Sarantos, C., and Crouse, D.T. (2021). Babinet's principle and saturation of the resonance frequency of scaled-down complementary metasurfaces. Appl. Phys. Lett. *118*, 221901.
45. Lu, Z., Xia, C., Zhang, Y., and Tan, J. (2023). Metasurface with Electrically Tunable Microwave Transmission Amplitude and Broadband High Optical Transparency. ACS Appl. Mater. Interfaces *15*, 29440–29448.

STAR★METHODS

KEY RESOURCES TABLE

REAGENT or RESOURCE	SOURCE	IDENTIFIER
Software and algorithms		
CST Studio Suite 2022	Dassault Systèmes	https://www.3ds.com
MATLAB	MathWorks Co., LTD	https://www.mathworks.com/products/matlab.html; RRID: SCR_001622

RESOURCE AVAILABILITY

Lead contact

Further information and requests for resources and reagents should be directed to and will be fulfilled by the lead contact, Ling Wang (wangling@hnfnu.edu.cn; lingwangbupt@foxmail.com).

Materials availability

This study did not generate new unique reagents.

Data and code availability

(1) Data reported in this paper will be shared by the lead contact upon request.
(2) This paper does not report original codes.
(3) Any additional information required to reanalyze the data reported in this paper is available from the lead contact upon request

EXPERIMENTAL MODEL AND SUBJECT DETAILS

The CST Microwave Studio software has been employed to analyze the near-field distribution and the far-field pattern of the metasurface. VO_2 is simulated based on the Drude model.

METHOD DETAILS

Simulate the devised unit cell in the CST Studio Suite 2022. Apply the Frequency Domain Solver. Set boundary conditions as the unit cell in the *x*- and *y*-directions. Set Floquet ports in the *z*-direction. The port excitation is the CP plane wave. Simulate the devised tunable metasurface carpet cloak, the bared triangular metal bump, and the virtual objects in the CST Studio Suite. Apply the Time Domain Solver. Set the boundary conditions as periodic in the *y*-direction and open in the *x*- and *z*-directions. CP plane waves illuminate the metasurface, metal bump, and virtual objects along the $-z$-direction with different polar angles. The metal is Au with a conductivity of 4.561×10^7 S/m and the dielectric layer is SiO_2 with a relative permittivity of 3.8. VO_2 is simulated based on the Drude model with $\varepsilon_\infty = 12$, $\omega_p{}^2\,(\sigma_0) = 1.4 \times 10^{15}$ rad/s, $\sigma_0 = 3 \times 10^3\ \Omega^{-1}\mathrm{cm}^{-1}$, and $\gamma = 5.75 \times 10^{13}\ \mathrm{s}^{-1}$. For VO_2 in the state of insulation or metal, set σ to 200 S/m or 2×10^5 S/m respectively. The switching of the VO_2 state could be realized by heating.

QUANTITATION AND STATISTICAL ANALYSIS

The simulation data is produced by CST Microwave Studio software. Figures shown in the main text were produced by Origin and Microsoft Visio from the raw data.

ADDITIONAL RESOURCES

Any additional information about the simulation and data reported in this paper is available from the lead contact on request.